SENIOR SEMINAR PAPER

Testing Analysis Algorithms for the $^2\text{H}(\text{e}, \text{e}'\text{p})\text{n}$ Reaction

Author:
C. A. COPOS
Department of Physics
University of Richmond

Research Advisor:
Dr. G. P. GILFOYLE
Department of Physics
University of Richmond

A senior thesis submitted to the faculty of the
University of Richmond
in partial fulfillment of the requirements for the degree of
Bachelor of Science.

April 12, 2010

Acknowledgments

Abstract

We have measured the asymmetry $A_{LT}\prime$ of the ^{2}H(e, e'p)n reaction in quasielastic kinematics at a beam energy of 2.56 GeV over a 4-momentum transfer range $Q^2 = 0.2 - 2.0 (GeV/c)^2$ with the CLAS detector at Thomas Jefferson National Laboratory. We have performed a Monte Carlo simulation of the reaction in order to test the analysis code used to extract $A_{LT}\prime$ associated with the fifth structure function. The Hulthen distribution was used to select the magnitude of the internal Fermi momentum of the target nucleon and the direction was chosen isotropically. The direction and Fermi momentum of the target nucleon were weighted by integrating the elastic cross section in the frame of reference of the moving nucleon over the CLAS acceptance. A fit to the measured $A_{LT}\prime$ was incorporated into the Monte Carlo simulation to model the fifth structure function. The GEANT3-based code GSIM was used to simulate the CLAS detector. Monte Carlo events were analyzed with the same code used to extract $A_{LT}\prime$ from the experimental data. We simulated quasielastic scattering at a beam energy of 2.56 GeV using two polarities of the CLAS toroidal magnet. The asymmetry extracted from Monte Carlo events is consistent with the input function for the asymmetry within the uncertainties of the calculation[1].

Keywords: JLAB, CLAS, asymmetry, Hulthen distribution, deuteron nucleus, elastic differential cross section.

Contents

List of Figures

List of Tables

Part I. Scientific Background

1 Modern Atomic Physics

Modern Atomic Physics began at the turn of the 19th century with the discovery of the fundamental building blocks of matter: electrons, nuclei, ions, photons, and their interactions. The idea that all matter is composed of smaller fundamental building blocks can be traced back to the Greek philosophers Democritus and Leucippus. This early philosophical concept of atom was contrary to the *continuum hypothesis* embraced by Aristotle, which viewed matter as continuous and therefore divisible without limit. At the beginning of the 20th century, important advancements were made that supported the atomos hypothesis. In 1808 John Dalton used the concept of atoms to show that when chemical elements combine, they do so in a ratio of small whole number[2]. For example, carbon and oxygen react to from carbon monoxide CO or carbon dioxide CO_2, but not $CO_{3.14}$.

With the development of accelerators and particle detectors, physicists have the tools needed to delve deeper into the structure of the nucleus and, finally, the elementary particles. The current picture is that matter is made up of a combination of quarks, leptons, and force carriers. The most widely accepted theory of elementary particle physics at present is the Standard Model.

2 An Introduction to the Standard Model

The Standard Model is a theory of three of the four known fundamental interactions and the elementary particles that take part in these interactions. The first step towards the Standard Model was Sheldon Glashow's discovery of a way to combine the electromagnetic force and the weak interaction, most commonly observed in beta decay[3]. The model includes 12 elementary particles of spin $\frac{1}{2}$ known as fermions, as depicted in Figure 1 [1]:

Fermions can be further categorized as a quark or a lepton by how they interact with other elementary particles. A quark is an elementary particle with non-whole number electric charge and unlike the leptons, they interact via the strong or color force. A lepton is also an elementary particle but with whole number electric charge and they interact via the electromagnetic force or via the weak interaction.

The model also includes four force mediating particles that have spin 1: photons who mediate the electromagnetic force between electrically charge particles, the Z^0 and $W^{\pm}$ bosons who mediate the weak interactions between quarks and leptons, and gluons who mediate the strong nuclear interaction between quarks, commonly observed as the force that binds protons and neutrons together to form a nucleus.

The Standard Model has correctly predicted the existence of $W^{\pm}$ and Z^0 bosons, as well as the top and charm quarks before the particles were observed [1]. Their predicted properties were experimentally confirmed with good precision. For example, the Table 1 compares the measured masses of the $W^{\pm}$ and Z^0 bosons with the masses predicted by the Standard Model:

---

[2] Dalton's Law of Multiple Proportions;
[3] Type of radioactive decay in which an electron or a positron is emitted;
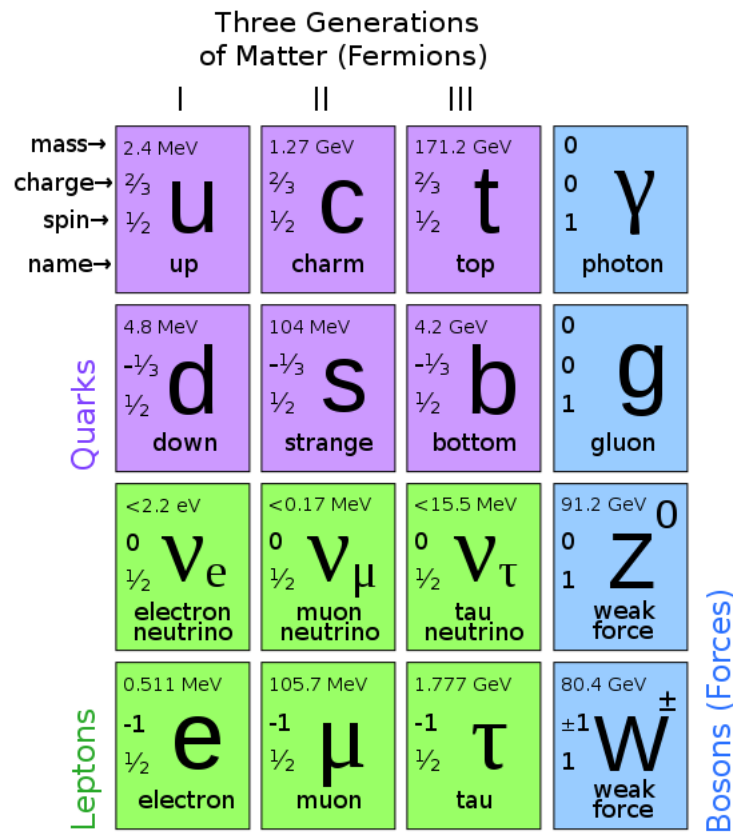
Fig. 1: The Standard Model.

The Standard Model, though it still contains several open questions such as why neutrinos have masses, has been very successful in predicting the structure of matter at the smallest scale. We know that the atomic nucleus is made up of protons and neutrons bound by the strong nuclear force. We have experimentally observed that quarks are confined inside the nucleons[4], but have also observed that nucleons are not confined [4]. Therefore, we would like to better understand what forces hold quarks together. The Standard Model groups two extant theories that have been developed to describe the behavior and interactions of quarks: The Hadronic Model and the theory of Quantum Chromodynamics.

---

[4] Collective name for neutrons and protons;

Quantity	Measured (GeV)	Standard Model Prediction (GeV)
Mass of W boson	80.398 ± 0.025	80.373 ± 0.023
Mass of Z boson	91.1876 ± 0.0021	91.1874 ± 0.0021

Tab. 1: Predicted and measured masses of the W and Z bosons [2, 3].

3   Theories of Quark Interactions

The Hadronic Model deals with the interactions between hadrons (particles made up of groups of two or three quarks bound together by the strong nuclear force) at low energies[5] in which nuclei can be approximated as collections of protons and neutrons. This is the strong force, the residual force between quarks. Figure 2 demonstrates the success of the Hadronic Model at low energies [6]. The plot shows the intensity pattern or cross section from a scattering experiment together with previous SLAC[6] data and theoretical calculations. The quantity on the horizontal axis is the square of the four-momentum transfer, Q^2, (a relativistic space-time analog of the classical momentum transfer) over a range of 0.5 - 6.5 GeV[7]. The quantity on the vertical axis is the cross section that describes the probability of interaction in a two-particle initial state. The error bars represent statistical and systematic uncertainties added in quadrature. Note that the experimental data points agree very well with the Hadronic Model calculation by Van Orden, et al. (dotted line) covering five orders of magnitude as shown below:
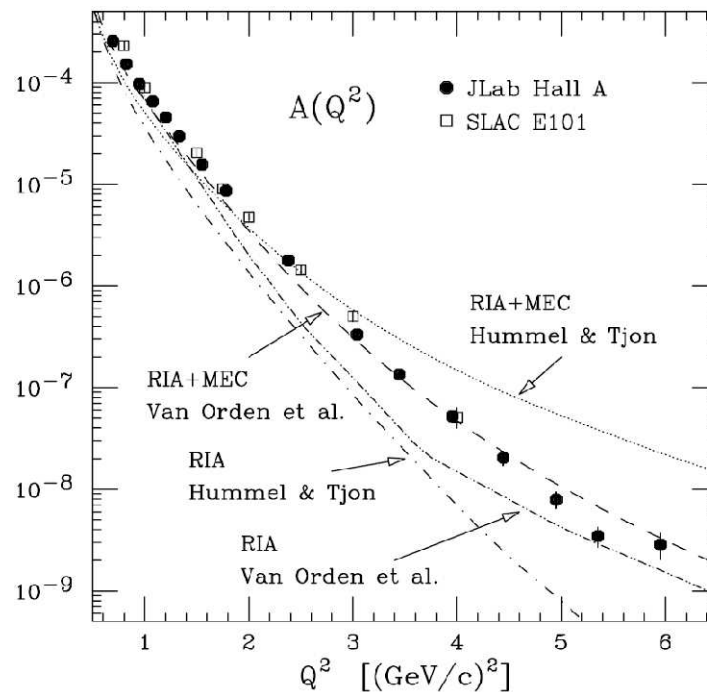

Fig. 2: Cross section as a function of four momentum transfer: Hadronic Model. The Hadronic Model correctly explains the behavior of quarks at low energies.

[5] For our purposes, this means $O(1)$GeV;
[6] Stanford Linear Accelerator Center;
[7] In natural units;

Quantum Chromodynamics, QCD, is a theory of the color force, describing the interactions of the quarks and gluons making up hadrons. QCD predicts a property known as asymptotic freedom: at very high energies, quarks and gluons behave like free non-interactive particles (except for the Coulomb force) [7]. Another feature of the theory is confinement, meaning that at large distances (~ 0.5 fm) the force between quarks does not decrease as they separate but rather stays the same, equal to 14 tons. QCD is a correct theory of quark interactions, but has been unproductive in the sense that it is extremely difficult to use the theory to make quantitative accurate predictions at energy scales we are capable of creating. At high energies, $O(100)$GeV, QCD is very successful [7]. Figure 2 demonstrates the success of QCD; it shows the cross section for proton-antiproton collisions as a function of E_T, the transverse energy flow. There is very good agreement between the calculated curves (resulting from perturbative[8] QCD calculations) and the data points:
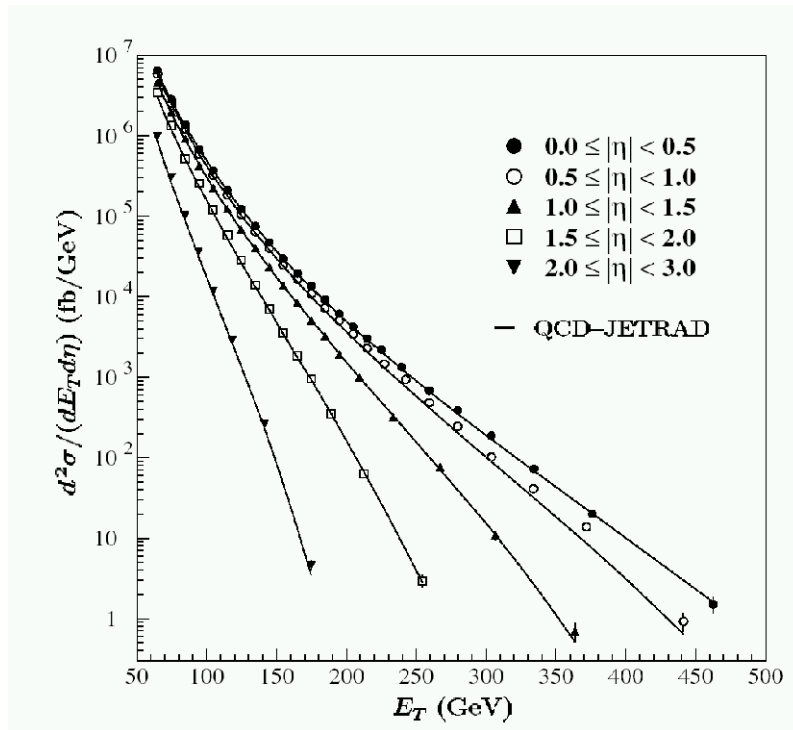
Fig. 3: Cross section as a function of transverse energy: QCD Model [7]. The QCD Model correctly explains the behavior of quarks at high energies.

Note the large differences in the energies scales on the horizontal axes of Figures 2 and 3. Though the two models described above have been validated experimentally we do not have a transition model; a model that explains the physical behavior at the energies in between these extremes. Figure 4 depicts the poorly understood transition from the nucleon picture to the quark model of QCD [8]. This figure shows a measurement of the deuterium tensor polarization observable t_{20},

---

[8] This is a style of calculation where one sums series of progressively smaller terms. [5] provides a very good introductory discussion of the computational methods of perturbative QCD, pQCD;

which is related to the differential cross section of deuterium[9], as a function of Q^2 at a low energy range. As expected, the data points are in good agreement with theoretical predictions of the Hadronic Model (dotted lines). However, the theoretical QCD prediction (full line), extrapolated from high Q^2 to low Q^2, fails to reproduce the data points at the low Q^2 range. According to [9, 10] it is expected that the transition will occur in the GeV region.
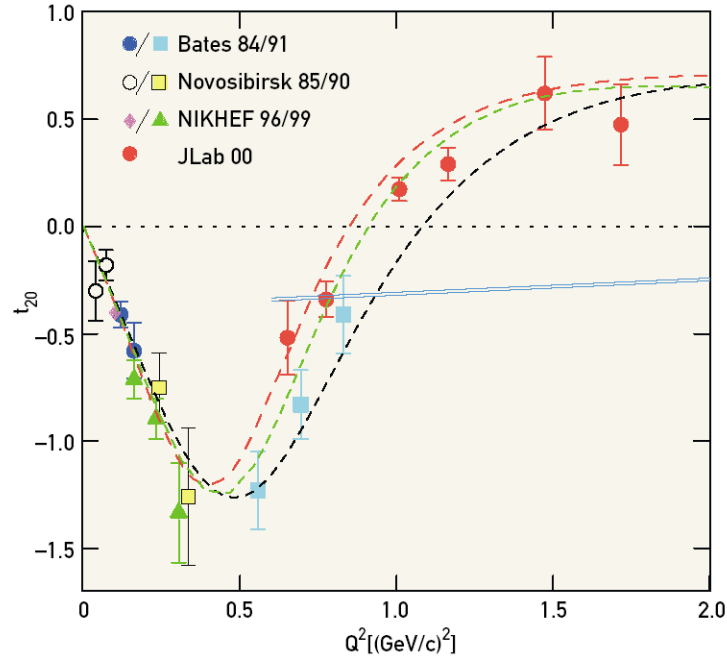
Fig. 4: Predictions for QCD at low range energies [8]; the blue line indicates the QCD prediction for low Q^2. An ultimate goal of nuclear physics is to better understand the behavior of quarks at the intermediate energies.

4   Physical Situation

A quantitative understanding of the structure of the deuteron, the nucleus of deuterium[10] and the simplest nuclear system composed of a two-nucleon bound state, has long been considered an important testing ground for the two models described above: the model of the short range nuclear interaction and the explicit influence of quark degrees of freedom. In order to study the structure of the deuteron, an experiment was carried out in the CEBAF Large Acceptance Spectrometer (CLAS) in Hall B at Jefferson National Laboratory in Newport News, Virginia. The experiment

---

[9] The reader will find that reference [8] contains a detailed mathematical explanation of the relationship between t_{20} and the cross section;

[10] Deuterium, ^{2}H, is a stable isotope of hydrogen and contains one proton and one neutron;

was an electron scattering off of a deuteron and detecting a proton, with the neutron as the residual nucleus, at an energy of 2.56GeV.

Our interest is to measure an asymmetry to reveal useful information about the wave function of the deuterium nucleus. This is a key to our better understanding of the transition between the quark-gluon picture and the nucleon model.

5   Objective

The physical goal of this project is to measure the a largely unknown component of the deuteron wave function, known as the fifth structure function, a term of the cross section of ^{2}H(e, e'p)n, where ^{2}H denotes the deuterium atom, e is the incident electron, e' is the scattered electron, p is the scattered proton, and n is the residual neutron. No measurement of this term exists in this energy range so this experiment explores new territory of the strong nuclear force.

6   Procedure

We describe here how we performed a computer simulation of the ^{2}H(e, e'p)n reaction in order to test the analysis code used to extract the term of the cross section. To explain the procedure in a cogent manner, this paper is organized into four main sections. *Experimental Background* presents the experimental setup and technique. *Mathematical Work* provides the mathematics and kinematics analysis leading up to the program. *Computational Work* presents a description of the programs used and the methodology, and *Results* provides the results of our research.

Part II. Experimental Background

The experiment was conducted at Thomas Jefferson National Accelerator Facility (JLAB) in Hall B using the Continuous Electron Beam Accelerator Facility (CEBAF) Large Acceptance Spectrometer (CLAS). Jefferson Lab, a Department of Energy National Laboratory, was designed to study the structure of the atomic nucleus, specifically the interaction of the quarks that make up protons and neutrons. It is comprised of a large electron accelerator, CEBAF, and three experimental research halls: Halls A, B, and C. The experiments conducted are dedicated to pursue the study of the three main research topics: the structure of the nucleus, the structure of nucleons, and probing the Standard Model's limits. By studying the critical mid-level range of energies[11], Jefferson Lab plays a critical role in developing our understanding of the transition between the Hadronic Model and the QCD theory.

---

[11] 2-6 GeV;

7   CEBAF

CEBAF is the large electron accelerator and the design consists of two linear accelerators that accelerate an electron beam, connected by arcs of bending magnets at each end. Electrons are directed around a racetrack-shaped loop of about 7/8 of a mile around, 25 feet underground. CEBAF is capable of producing electron beams with energies $2 - 6$ GeV, where the electron beam can travel around the accelerator up to five times near the speed of light. The CEBAF accelerator is based on superconducting accelerating cavities operating at a very stabilized frequency of 1.5×10^9 s [11]. The electrons ride on the crest of the accelerator radio frequency wave and then sent to one of the three halls where it collides with a target and the debris is measured by various detectors.

8   CEBAF Large Acceptance Spectrometer - CLAS

8.1   Introduction

CLAS is a collection of detectors located in the experimental Hall B at JLAB (Fig. 5). The CLAS spectrometer is designed to measure and identify the debris from a nuclear reaction. The detector is unique in that it has a very large acceptance; that is to say, it can measure the momentum and angles of almost all particles produced in the collisions regardless of the scattering angle. Roughly spherically shaped, the detector measures 30 feet across and weighs 45 tons. It completely surrounds the target with successive layers of different types of particle detectors.
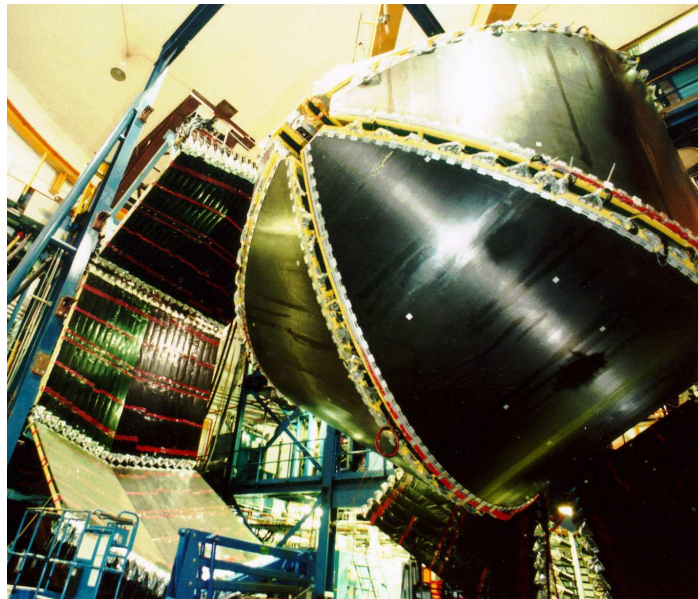

Fig. 5: The CLAS detector [11].

8.2   Detector Components

CLAS is a six sector magnetic spectrometer with a near 4π solid angle coverage. CLAS consists of six independent magnetic spectrometers each instrumented with drift chambers, time-of-flight (TOF) scintillators covering polar angles $8° < \theta < 143°$, a gas-filled threshold Cerenkov counter (CC), and a lead-scintillator sandwich-type electromagnetic calorimeter (EC) covering $8° < \theta < 45°$ [6]. A toroidal magnet is used to measure charged particle momentum. With the aid of electrical signals produced by each detecting element, each collision is reconstructed and the intensity pattern reveals the forces at play in the particle collision. Figure 6 is a cross section view of the CLAS detector, where each of the component detectors is visible and labelled. We will now proceed to describe in greater detail each of the component particle detectors.
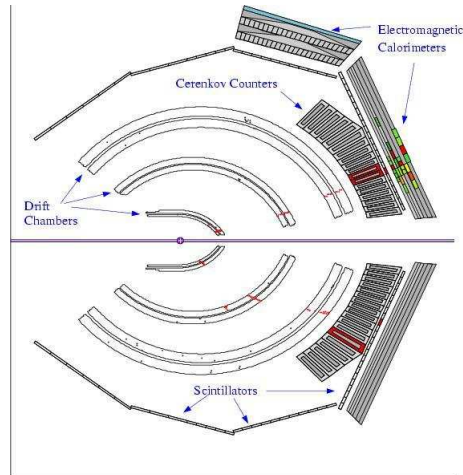
Fig. 6: A cross section view of the CLAS detector [6].

A toroidal magnet, situated around the electron beam in CLAS, causes charged particles to bend as they pass through. The magnetic field generated by the toroidal magnet has two polarity settings: normal, electrons are in-bending, and reversed, electrons are out-bending. We can set the magnitude of the field by changing the current.

A drift chamber (see Fig. 6) is a detector for particles of ionizing radiation. It is an advanced form of the Geiger counter which detects not only the presence of radiation but also its location [12]. It is a large volume filled with positively charged wires and with a chosen gas. As the charged particle traverses the chamber, it ionizes the atoms in the gas and displaced electrons drift towards the positively charged wires. This creates an electric signal. The pattern of hits is used to reconstruct the trajectory of the particle. As the particle bends in the CLAS magnetic field, one can use the pattern of hits to measure the momentum.

Time-of-flight (TOF) (see Fig. 6) scintillators can differentiate between a lighter and a heavier particle with the same momentum using the time from interaction to hitting the scintillator. It is made up of long scintillating bars, so that when an ionized particle passes through one of these bars, it emits light [12]. The light is then detected by a photo-multiplier tube, located at the end of each scintillating bar. The electron beam is pulsed meaning that it consists of a series of discrete

beam packets. We know when the beam packet strikes the target. Combined with the time when the scattered particle strikes the scintillator and the path length from the target (determined from the trajectory measured with the drift chambers) one can extract the particle velocity. With this velocity and the measured momentum (from the bending of the particle track in the CLAS magnetic field) one can extract the mass of the particle and identify it.

The Cerenkov detectors (see Fig. 6) are detectors that separate electrons from pions. The detector is composed of a gas which is optically thicker than air. The concept of the detector is based on Cerenkov radiation: a particle moving through the gas described above at a velocity above the speed of light in the gas emits electromagnetic radiation to reduce its speed in the medium [13]. While the electron emits light in the Cerenkov detector, the pion, a heavier particle moving at a speed less than the speed of light in the gas, does not emit Cerenkov radiation. A coincidence in the drift chamber and Cerenkov counter would, therefore, signify the presence of an electron.

Electromagnetic calorimeters (see Fig. 6) are the experimental apparatus that are used to measure the energy of the particles. They are the final layer in the CLAS detector and are made up of alternating layers of lead and scintillator. Particles interact in the lead creating a shower of particles that generate photons in the plastic scintillator. These photons are collected and the amount of light is proportional to the energy. For the purpose of this paper we will define an *event* when a particle triggers a signal from successive layers of the CLAS detector. Using the various detectors in CLAS we can determine the identity of a particle based on its trajectory, charge, momentum, energy, scattering angle, and velocity.

9   Experimental Setup

For the experiment two reactions were measured in the CLAS detector at the same time and from the same target to reduce systematic uncertainties. Two data sets were used at two electron-beam energies, 2.56GeV and 4.2GeV, with normal torus polarity, electrons bend towards the beam. A third data set at beam energy 2.56GeV, reversed[12] torus polarity, was conducted in order to reach a low Q^2. Our research uses the data set at 2.56GeV for both normal and reversed torus polarity in order to cover a broader Q^2 range.

The target nucleus was deuterium. A dual cell target was used consisting of two collinear cells each 5 cm long - one filled with ^{1}H and one with ^{2}H - and separated by 4.7 cm. The CLAS resolution of 2 mm enabled us to separate the events from different targets [21].

Part III. Mathematical Analysis

Electron scattering from a deuteron is a crucial tool in understanding the internal structure and dynamics of the nuclear two-body system [14]. In particular, for this research it is an ideal testing ground for the models of the nuclear force as described in the Hadronic Model and the quark-gluon picture in the framework of QCD. Our physical objective is to measure the fifth structure function, one of the terms of the cross section of the ^{2}H(e, e'p)n reaction never before measured.

---

[12] Electrons bend away from the beam;

10   Kinematics Analysis

The cross section of the ^{2}H(e, e'p)n reaction with a polarized beam and unpolarized target has a component that is the imaginary part of the interference term between longitudinal and transverse parts of nuclear current. As featured in Figure 7, the longitudinal direction points in the direction of the exchanged photon, while the transverse direction is orthogonal to the longitudinal direction. The azimuthal angle ϕ_{pq} is the angle between the scattering and reaction planes, while the angle θ_{pq} is the angle between the longitudinal direction and the direction of the scattered proton. The angle θ_e is the angle between the incoming electron, $\vec{e}$, and scattered electron, $\vec{e'}$, and $\vec{q}$ denotes the three-momentum transfer. A discussion the importance of the angle ϕ_{pq} for the electron scattering of a deuteron nucleus will follow in *Analytical Approach*.
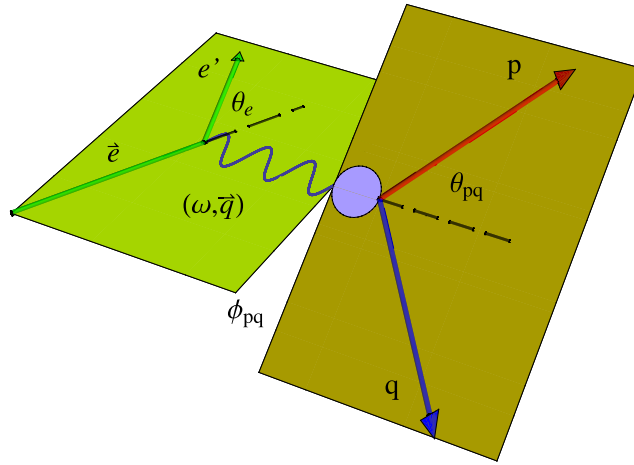
Fig. 7: Kinematics electron-deuteron scattering.

Another important feature of the kinematics of this experiment is the limitation of elastic events in our experimental calculations and simulations. In inelastic events, where kinetic energy is not conserved, the incoming particle often causes the nucleus it strikes to become excited or break. In our investigation of the transition between the Hadronic model and the QCD model, we are interested in elastic collisions where the conserved kinetic energy is exchanged between the electron and the deuteron nucleus via a virtual photon.

11   Analytical Approach

The differential cross section for elastic electron-deuteron scattering is described by the following formula,

$$\boxed{\frac{d^3\sigma}{d\omega d\Omega_e d\Omega_p} = \sigma^{\pm} = \sigma_L + \sigma_T + \sigma_{LT}cos(\phi_{pq}) + \sigma_{TT}cos(2\phi_{pq}) + h\sigma'_{LT}sin(\phi_{pq})} \tag{1}$$

where the right hand side of the equation represents the effective cross-section area in the longitudinal (L), transverse (T), and their cross terms: LT, TT, LT'. The electron beam is polarized with the spin of the electron is either aligned with the momentum of the beam, in which case the helicity of the beam $h = +1$, or the anti-aligned, $h = -1$. On the left hand side of the equation σ denotes the cross section, $d\omega$ is the infinitesimal element of the energy transfer, $d\Omega_e$ is the infinitesimal element of the electron solid angle, and $d\Omega_p$ represents the infinitesimal element of the proton solid angle.

The last term of the differential cross section equation $h\sigma'_{LT} sin(\phi_{pq})$ has rarely been measured. Note also that σ'_{LT} is the fifth structure function and it represents an unknown component of the deuteron wave function [14]. For most conventional detectors, the scattering plane is at the same angle as the reaction plane. However, the fifth term is nonzero only when the angle ϕ_{pq} is nonzero, and as a result in order to obtain a measurement of the entire cross section of the electron-deuteron scattering the detector must allow for out-of-plane measurements. As described in the *Experimental Background* section, the unique feature of CLAS offered the opportunity for out-of-plane measurements of the fifth term of the differential cross section.

To distinguish among the different models for the transition energy range, high precision is important. By considering a ratio of the cross-section terms, we reduce the vulnerability to systematic uncertainties because the correction terms cancel out [16]. Therefore we define the asymmetry function:

$$\boxed{A'_{LT} = \frac{\sigma'_{LT}}{\sigma_L + \sigma_T}} \tag{2}$$

By taking advantage of the orthogonality of the sine and cosine functions, as shown in *Appendix A*, we can express the asymmetry function as follows,

$$\boxed{A'_{LT} = \langle \sin(\phi_{pq}) \rangle_+ - \langle \sin(\phi_{pq}) \rangle_-} \tag{3}$$

where $\langle \sin(\phi_{pq}) \rangle_\pm = \frac{\sum_{data} \sin(\phi_i^\pm)}{N_\pm}$, a weighted average of $\sin(\phi_{pq})$.

Below, in Figure 8, are the preliminary plots of the extracted function A'_{LT} at a beam energy of 2.56 GeV with both normal (left panel) and reversed (right panel) magnetic torus polarity. The total systematic uncertainty is represented in red at the bottom of the plot and was obtained by adding the uncertainties for each cut in quadrature. p_m denotes missing momentum where $\vec{p_m} = \vec{q} - \vec{p_p}$ and q is the three-momentum transfer and p_p is the ejected proton momentum. The asymmetry shows clear and statistically significant variation with p_m with maximum magnitude of 4-7
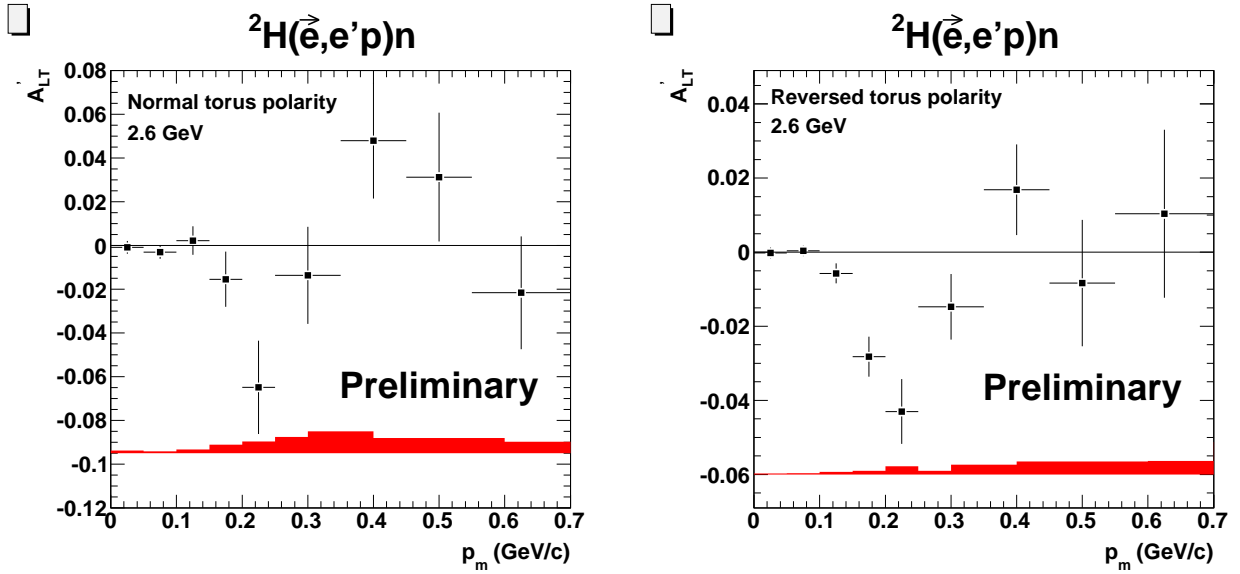
Fig. 8: Extracted asymmetry function varying over missing momentum.

In the following section, *Computational Work*, we describe how we performed a computer simulation of the ^{2}H(e, e'p)n reaction in order to test the analysis code used to extract the asymmetry function.

Part IV. Computational Work

For the computationally intensive simulations and data analysis of the ^{2}H(e, e'p)n reaction and the CLAS detector components, the Supercomputing Cluster at the University of Richmond was used. It consists of one master node and 52 slave nodes of which 49 are dual 1.4 GHz Athlon class and 3 are 2.0 Ghz Athlon class [18]. The computing cluster runs on Linux operating system and uses the Beowulf system for managing batch jobs. Programs are written in Fortran, Perl, and C++ and are submitted to the master node. When received, the master node then sends the commands to the slave nodes who execute the jobs. A series of programs were employed to simulate CLAS detectors and to extract the asymmetry function from the events generated.

12   Program Description

Developed and managed by CERN[13], the GEANT3[14] program was initially developed for high energy physics experiments but it has found applications also outside this domain in the areas of medical and biological sciences, and astronautics. The program described the passage of elementary particles through matter. The primary applications of GEANT3 in nuclear physics are to track
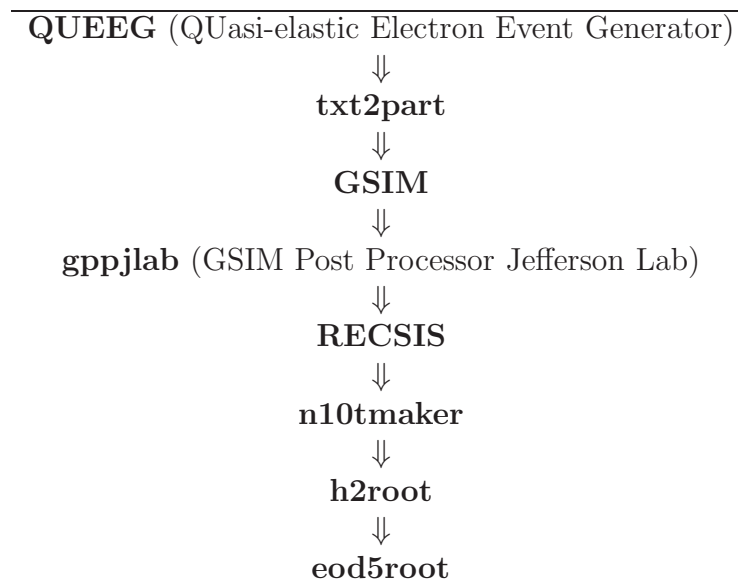
---

[13] European Organization for Nuclear Research;
[14] Acronym stands for "GEometry ANd Tracking";

particles through an experimental setup for simulation of detector response, and it can be used to generate a graphical representation of the setup and of the particle trajectories.

GSIM is another program used specifically for the CLAS detector at Jefferson Lab. The package uses the GEANT routines from the CERN libraries as a framework for a Monte Carlo simulation of the CLAS detector. This is the main simulation program used in our simulation sequence of the reaction in the CLAS detector. These simulation packages are essential to our experimental research so we can measure the response of our detector.

13   Simulation Sequence

Table 3 contains an overview of the sequence of programs used to simulate a reaction in CLAS. In the simulation and analysis process, two event data banks are used: the "PART" bank contains the thrown events that are generated by QUEEG before they are passed through the CLAS simulation GSIM, and "EVNT" bank represents the events that actually made it through the detector and the analysis codes. A summary of the scripts used to simulate and analyze the data is given below.

QUEEG (QUasi-elastic Electron Event Generator)
⇓
txt2part
⇓
GSIM
⇓
gppjlab (GSIM Post Processor Jefferson Lab)
⇓
RECSIS
⇓
n10tmaker
⇓
h2root
⇓
eod5root

Tab. 2: The simulation sequence.

- **QUEEG**, generates quasi-elastic electron events by creating electron 4-vectors;

- **txt2part**, converts the QUEEG output files into BOS files (PART bank events);

- **GSIM**, the main Monte Carlo simulation program;

- **gppjlab**, makes the GSIM output look more like real data by knocking out dead scintillators and wires and adding some Gaussian smearing to the data;

- **RECSIS**, the standard program for reconstruction of CLAS data written mostly in FOR-TRAN. It acts as a shell for analyzing CLAS BOS-based data;

- **n10tmaker**, converts EVNT and PART BOS files (the output of RECSIS) into hbook ntuples (the input of h2root);

- **h2root**, converts hbook ntuples into ROOT ntuples;

- **eod5root**, a ROOT program that allows the user to extract histograms from the output of h2root and any other final analysis components.

14   Monte Carlo Methods

Monte Carlo methods provide approximate solutions to a variety of mathematical and physical problems by performing statistical sampling experiments. In experimental nuclear physics, Monte Carlo methods are used for designing detectors, understanding their behavior, and comparing experimental data to theory. Monte Carlo methods, though they have different implementations, all follow the same steps [19]:

1. Define a domain of possible inputs;

2. Generate inputs randomly from the domain using a certain probability distribution;

3. Perform a deterministic computation using the inputs;

4. Aggregate the results of the individual computations into the final result.

There are two main reasons why scientists use Monte Carlo methods: anti-aliasing property, that is to say the ability to randomly generate inputs (therefore no systematic uncertainties), and ability to approximate quickly an answer. To exemplify the process of a Monte Carlo calculation we include Figure 9 [20]. It shows how a triangular distribution with a minimum value of 1, maximum of 8 and most likely value of 4 is recreated as we iterate through the simulation process. At the first iteration, only one value has been randomly selected between the limits of the distribution. However, after 100 iterations it can be seen that values around the most likely value, 4 have been selected more frequently than those at the extremes. Finally, after 5000 iterations the triangular distribution can be observed to be sufficiently recreated with the majority of the samples selected around the most likely value with values spreading out towards the extremes sampled with decreasing frequency.
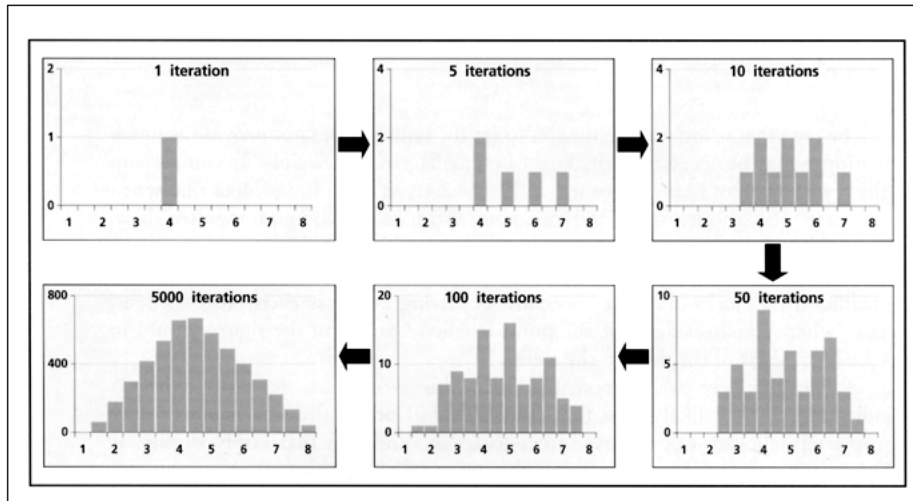
Fig. 9: Monte Carlo Simple Distribution Example [20].

In this example only one parameter is shown, but this idea can easily be extended to include several distributions. Our physical goal is to test the analysis algorithm used to extract the asymmetry from the reversed and normal polarity 2.56 GeV beam energy data sets. GSIM, the simulation package used for CLAS simulations, uses a very similar idea to generate events. Using the experimentally measured asymmetry instead of the "triangular distribution" and several other properties of the experiment, we generate events in CLAS and analyze them with the same analysis code used to extract the experimentally measure asymmetry. We will now address further methods employed and discuss in detail how we are able to generate events similar to the experimental features of the ^{2}H(e, e'p)n reaction.

15   More Computational Methods

As illustrated in the simple triangular distribution Monte Carlo experiment, for the simulation we need a certain probability distribution which the simulated events will follow. Using the analysis code we extracted the asymmetry function for both polarities of the torus magnet and fit it to two polynomial equations, as shown in Figure 10.
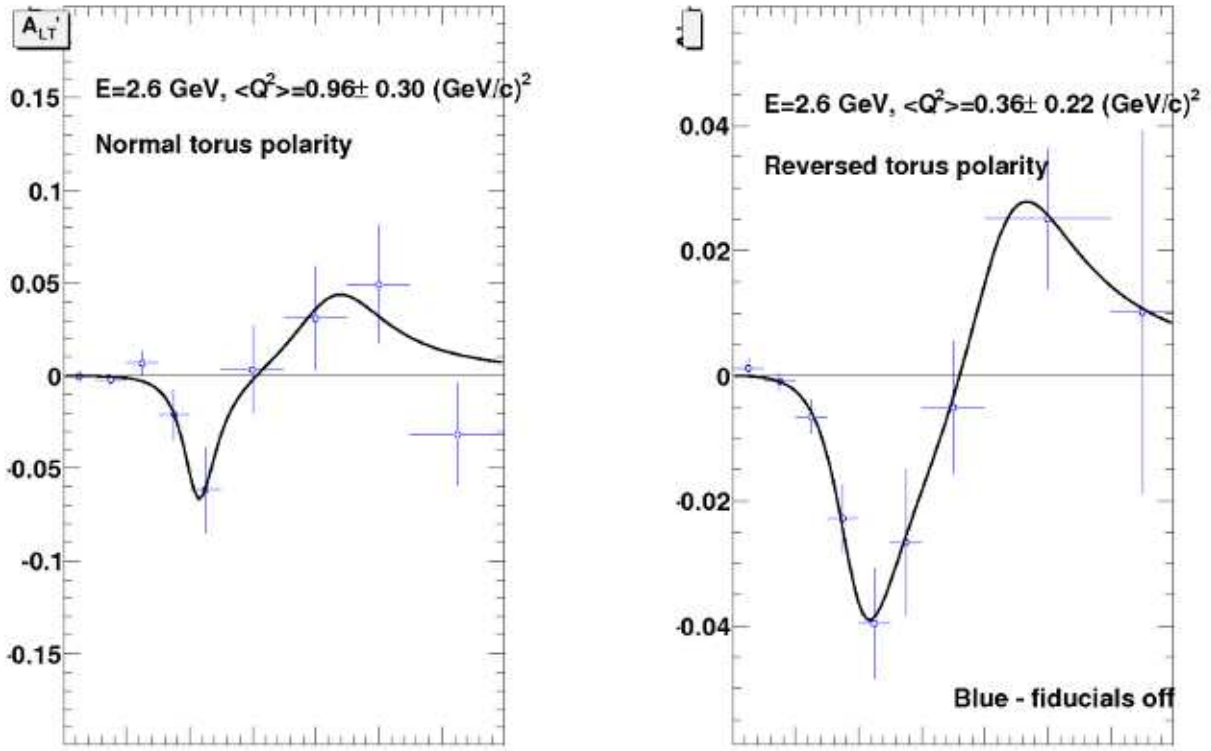
Fig. 10: Polynomial fits to the asymmetry function.

For the normal torus polarity data set (left panel of Fig. 4.2) the equation used to fit the measured asymmetry is:

$$f(x) = \frac{\delta_1 x^2 + \delta_2 x^4}{1 + \delta_3 x + \delta_4 x^2 + \delta_5 x^4 + \delta_6 x^6} \tag{4}$$

where $\delta_1 = -0.0344$, $\delta_2 = 0.3204$, $\delta_3 = -11.1479$, $\delta_4 = 35.4709$, $\delta_5 = -119.206$, and $\delta_6 = 227.042$. For the reversed torus polarity data set (right panel of Fig. 4.2) the equation used to fit the measured asymmetry is:

$$f(x) = \frac{\epsilon_1 x^2 + \epsilon_2 x^4}{1 + \epsilon_3 x + \epsilon_4 x^2 + \epsilon_5 x^4 + \epsilon_6 x^6} \tag{5}$$

where $\epsilon_1 = -0.0653$, $\epsilon_2 = 0.5031$, $\epsilon_3 = -11.0388$, $\epsilon_4 = 36.0937$, $\epsilon_5 = -126.685$, and $\epsilon_6 = 256.143$.

Another distribution included in the Monte Carlo simulation is the momentum distribution of the target nucleon, the neutron in the deuteron nucleus. A well known distribution was used, the Hulthen distribution, to select the magnitude of the internal Fermi momentum of the neutron and the direction was chosen isotropically. The direction and Fermi momentum of the target nucleon

were weighted by integrating the elastic cross section in the frame of reference of the moving nucleon over the CLAS acceptance. A graph of the Hulthen momentum distribution is shown in Figure 11. [21],
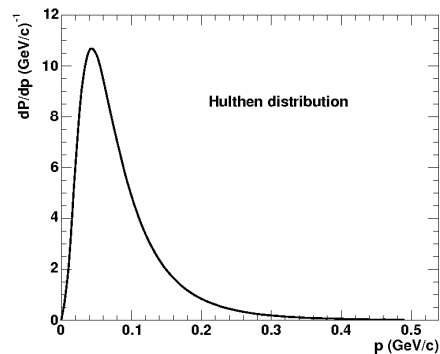

Fig. 11: Hulthen momentum distribution.

However in some instances the process of selecting the internal Fermi momentum would give high uncertainties in the simulated events. Therefore at high p_m, missing momentum, we changed our process of selecting the internal Fermi momentum to increase the minimum of the probability distribution to get more events in that range. We generated a plot showing the thrown events and the simulated ones so that we could account for the resolution effects in the simulated ones. Figure 12 shows the resolution effects for high momentum for just a few events. The simulated events shown in the red curve, are compared to the thrown events, shown in the blue curve. Notice that the smearing of the events in the simulation spreads out those events (red curve) so they extend below the minimum p_m at $p_m = 0.35$ GeV. As expected, the events of the simulation (red curve) is below the throw events (blue curve).
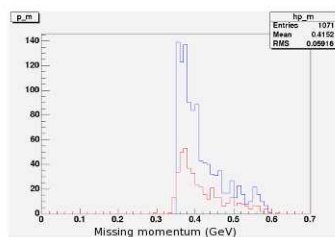

Fig. 12: Resolution effects for p_m. The vertical axis represents counts and the horizontal axis is the missing momentum measured in GeV.

Thus, we were able to achieve better statistics for high p_m. The fits to the measured A'_{LT}, described above, were incorporated into the Monte Carlo simulation to model the fifth structure

function. Next, we performed a Monte Carlo simulation of CLAS using GSIM and analyzed the generated events with the same analysis code used to extract the measured asymmetry.

Part V. Results

Our results are shown in Figure 13:
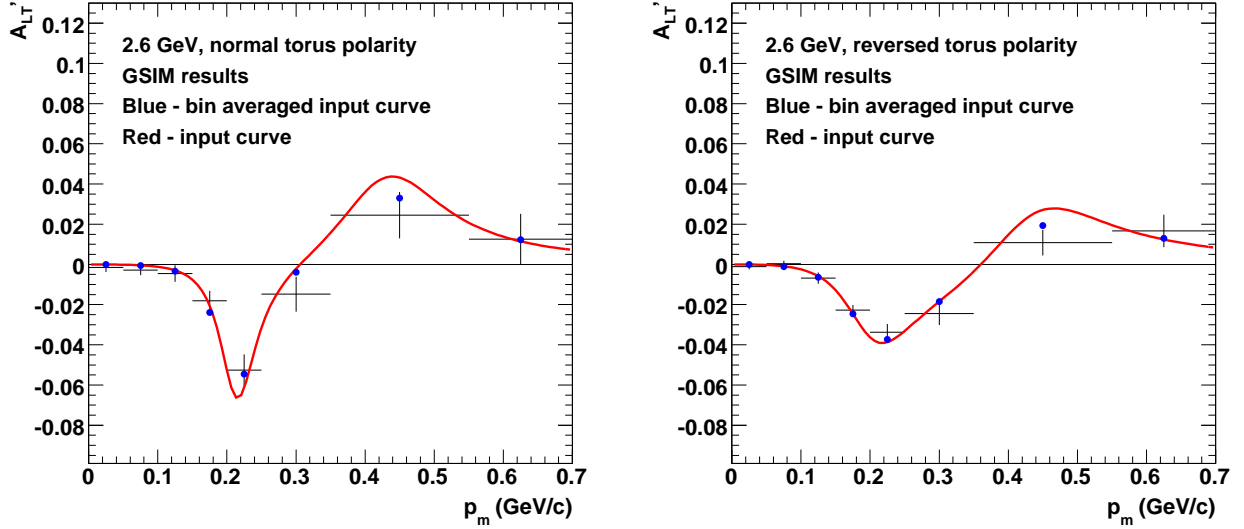
Fig. 13: Simulated asymmetry (red curve) with the results of the analysis.

The black points are the results of the simulation for the two torus polarity settings, while the blue points are the bin-averaged input asymmetry (red curve). Notice that the black and the blue points agree within the statistical uncertainties of the simulation. In order to achieve low uncertainties, we performed 22 runs each with 100, 000 events (each run took approximately 24 hours). To properly compare the simulated asymmetry with the results of the analysis , we averaged over the bins using the equation below,

$$\langle A'_{LT}\rangle_i = \frac{\int_{bin} A'_{LT}(p_m)\,dp_m}{\int_{bin} dp_m} \tag{6}$$

In order to assess the validity of our analysis code, we used reduced χ^2 as defined below,

$$\chi^2 = \frac{1}{n}\sum_{data}\frac{(y_i - f(x_i))^2}{\sigma_{y_i}} \tag{7}$$

where y_i are the bin averaged input points, $f(x_i)$ are the results of the simulation, σ_{y_i} is the uncertainty in y_i, and n represents the degrees of freedom, in our case, the number of data points. Reduced χ^2 for the reversed torus polarity data set is 1.0678 and for the normal torus polarity 1.0728. The reader should note that Appendix E includes the detailed calculation of reduced χ^2.

Part VI. Conclusions

The strong force is the fundamental force underlying the dynamics of the nuclear constituents in the nuclear medium. It is believed that the strong interaction is described within the framework of QCD, the fundamental quantum field theory, in which gluons act as facilitators of the interaction between quarks. However, it is not feasible to describe even the simplest nuclear system, the deuterium nucleus, starting from the basic equations of QCD. However, we have seen that the Hadronic Model of nuclear physics can be an effective and practical theory up to energies of a few GeV. Jefferson Lab plays a vital role in developing our understanding of the transition picture from the nucleon degrees of freedom to the quark-gluon ones. In order to study the transition from the Hadronic model at intermediate energies, an experiment was carried out using the CLAS detector in Hall B. The experiment was an electron scattering off of a deuteron detecting a proton, with the neutron as the residual nucleus, at an energy of 2.56GeV. Our interest is to measure an asymmetry to reveal useful information about the wave function of the deuterium nucleus.

We have performed a Monte Carlo simulation of the reaction in order to test the analysis code used to extract A'_{LT} associated with the fifth structure function, σ'_{LT}. As one can observe in Figure 11, the asymmetry extracted from Monte Carlo events is consistent with the input function for the asymmetry within the uncertainties of the calculation. This establishes the validity of the analysis algorithms used to extract A'_{LT} from the experimental data for the $^2H(e,e'p)n$ reaction.

References

[1] World Wide Web page of Wikipedia: http://en.wikipedia.org/wiki/StandardModel.

[2] K. Hagiwara et al. (Particle Data Group), Phys. Rev. D, *66*, 010001 (2002).

[3] CERN-EP/2001-098, hep-ex/0112021 (2002).

[4] *Measurement of the Neutron Magnetic Form Factor at High Q^2 Using the Ratio Method on Deuterium*, G. P. Gilfoyle, et al. (2007).

[5] B. Haynes, American Scientist, *96*, 450 (2008).

[6] L. C. Alexa, et al., Phys. Rev. Lett., *82*, 1374 (1999).

[7] B. Abbott, et al., Phys. Rev. Lett., *86*, 1707 (2001).

[8] D. Abbott, et al., Phys. Rev. Lett., *84*, 5056 (2000).

[9] S.Jeschonnek, Phys. Rev. C, *63*, 034609 (2001).

[10] *Opportunities in Nuclear Science: A Long Range Plan for the Next Decade*, DOE/NSF Nuclear Science Advisory Committee, April 2002, p. 30.

[11] World Wide Web page of Jefferson Laboratory Hall B: http://www.jlab.org/Hall-B/.

[12] World Wide Web page of COSY-11: http://ikpe1101.ikp.kfa−juelich.de/.

[13] World Wide Web page of Wikipedia: http://en.wikipedia.org/wiki/Cherenkovradiation.

[14] J. Lachniet, et al., Phys. Rev. Lett., *102*, 192001 (2009).

[15] P.Corvisiero et. al., Nuclear Instr. And Meth. *A346*, 433 (1994).

[16] *Out-of-Plane Measurements of the Structure Functions of the Deuteron*, G.P.Gilfoyle, W.K.Brooks, B.A.Mecking, S.Kuhn, L.Weinstein, M.F.Vineyard (2003).

[17] M.N.Rosenbluth, Phys. Rev. Lett., *79*, 615 (1950).

[18] World Wide Web page of G.P. Gilfoyle: https://facultystaff.richmond.edu/ggilfoyl/research/spiderwulf/clusterhome.html.

[19] World Wide Web page of Wikipedia: http://en.wikipedia.org/wiki/MonteCarlomethod.

[20] World Wide Web page of Food and Agriculture Organization of the United Nations: http://www.fao.org/docrep/009/a0238e/A0238E02.htm.

[21] World Wide Web page of G.P. Gilfoyle: https://facultystaff.richmond.edu/ggilfoyl/research/gmnCLASJun08.pdf.

Appendix A

This appendix will seek to explain in more detail the mathematical steps taken to deduce equation (2) in the *Analytical Approach* section, which relates A'_{LT} to σ'_{LT} and $\langle sin(\phi_{pq}) \rangle$. We start with the Rosebluth differential cross section for the deuteron nucleus,

$$\frac{d^3\sigma}{d\omega d\Omega_e d\Omega_p} = \sigma^{\pm} = \sigma_L + \sigma_T + \sigma_{LT} cos(\phi_{pq}) + \sigma_{TT} cos(2\phi_{pq}) + h\sigma'_{LT} sin(\phi_{pq}) \tag{8}$$

To isolate the σ'_{LT} term from the above equation we take advantage of the orthogonality of sine and cosine functions. For m and $n \in \mathbb{Z}$,

$$\int_0^\pi sin(n\phi_{pq}) sin(m\phi_{pq}) \, d\phi_{pq} = 0, \quad n \neq m \tag{9}$$

$$\int_0^\pi sin(n\phi_{pq}) sin(m\phi_{pq}) \, d\phi_{pq} = \pi, \quad n = m \tag{10}$$

$$\int_0^\pi sin(n\phi_{pq}) cos(m\phi_{pq}) \, d\phi_{pq} = 0, \quad \forall n, m \tag{11}$$

Using the above orthogonality relations and the trigonometric fact that the sinusoidal axis is centered at zero, the following can be easily verified:

$$\int_{-\pi}^\pi \sigma^{\pm} sin(\phi_{pq}) \, d\phi_{pq} = h\pi\sigma'_{LT} \tag{12}$$

In equation (5) observe how the only term surviving the integral on the right hand side of equation (1) is the fifth structure function term, σ'_{LT}. Now consider the following integral:

$$\int_{-\pi}^\pi \sigma^{\pm} \, d\phi_{pq} \tag{13}$$

Again using the fact that the sinusoidal axis is centered at zero observe that the following is true,

$$\int_{-\pi}^\pi \sigma^{\pm} \, d\phi_{pq} = 2\pi(\sigma_L + \sigma_T) \tag{14}$$

Putting equations (5) and (7), observe that we have obtained an equation for the weighted average of $sin(\phi_{pq})$,

$$\langle sin(\phi_{pq}) \rangle_{\pm} = \frac{\int_{-\pi}^\pi \sigma^{\pm} sin(\phi_{pq}) \, d\phi_{pq}}{\int_{-\pi}^\pi \sigma^{\pm} \, d\phi_{pq}} = \frac{h\pi\sigma'_{LT}}{2\pi(\sigma_L + \sigma_T)} = \pm\frac{\sigma'_{LT}}{2(\sigma_L + \sigma_T)} \tag{15}$$

And finally, these weighted averages can be combined to yield A'_{LT}:

$$\langle sin(\phi_{pq})\rangle_+ - \langle sin(\phi_{pq})\rangle_- = \frac{\sigma'_{LT}}{2(\sigma_L + \sigma_T)} - \frac{-\sigma'_{LT}}{2(\sigma_L + \sigma_T)} = \sigma'_{LT}(\sigma_L + \sigma_T) = A'_{LT} \qquad (16)$$
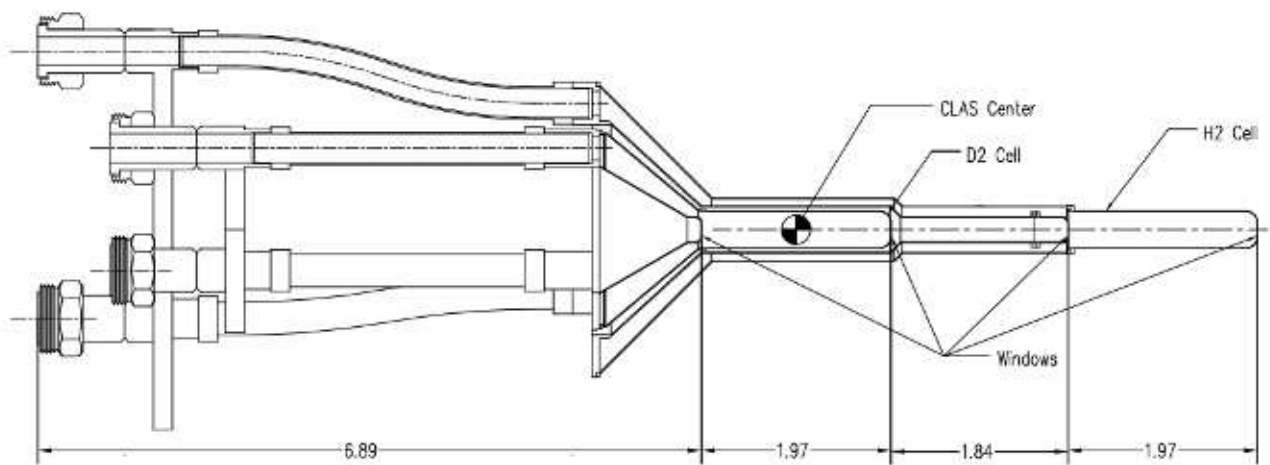
Appendix B

Fig. 14: Primary drawing of the E5 dual cell.

Appendix C

Root script for adding reversed field data points. A similar script exists for adding normal field data points.

```
//ROOT SCRIPT FOR ADDING REVERSED FIELD DATA POINTS    acc  7/31/09//
/////////////////////////////////////////////////////////////////////

TFile  *file1  =  new  TFile("summed_simevnthists1.root");  //  run1
TFile  *file2  =  new  TFile("summed_evnt2-7.root");   //run2
TFile  *file3  =  new  TFile("summed_evnt8-10.root");   //run3
TFile  *file4  =  new  TFile("summed_simevnthists11.root");   //run4
TFile  *file5  =  new  TFile("summed_simevnthists12.root");   //run5

Double_t  p_m_bin_edges
    [13]={0.0,0.05,0.10,0.15,0.20,0.25,0.35,0.55,0.70,1.0,1.25,1.5,2.0};
Int_t  n_varp_mbins  =  12;

//copy  run1

TH1F  *hp_m_sin_phi_plusrun1  =  new  TH1F("hp_m_sin_phi_plusrun1","",
    n_varp_mbins, p_m_bin_edges);
TH1F  *hp_m_unwgt_plusrun1  =  new  TH1F("hp_m_unwgt_plusrun1","",
    n_varp_mbins, p_m_bin_edges);
TH1F  *hp_m_sin_phi_minusrun1  =  new  TH1F("hp_m_sin_phi_minusrun1","",
    n_varp_mbins, p_m_bin_edges);
TH1F  *hp_m_unwgt_minusrun1  =  new  TH1F("hp_m_unwgt_minusrun1","",
    n_varp_mbins, p_m_bin_edges);

file1 ->cd();
file1 ->GetObject("hp_m_sin_phi_plus4","hp_m_sin_phi_plusrun1");
file1 ->GetObject("hp_m_unwgt_plus4","hp_m_unwgt_plusrun1");
file1 ->GetObject("hp_m_sin_phi_minus4","hp_m_sin_phi_minusrun1");
file1 ->GetObject("hp_m_unwgt_minus4","hp_m_unwgt_minusrun1");

//copy  run2


TH1F  *hp_m_sin_phi_plusrun2  =  new  TH1F("hp_m_sin_phi_plusrun2","",
    n_varp_mbins, p_m_bin_edges);
TH1F  *hp_m_unwgt_plusrun2  =  new  TH1F("hp_m_unwgt_plusrun2","",
    n_varp_mbins, p_m_bin_edges);
TH1F  *hp_m_sin_phi_minusrun2  =  new  TH1F("hp_m_sin_phi_minusrun2","",
    n_varp_mbins, p_m_bin_edges);
TH1F  *hp_m_unwgt_minusrun2  =  new  TH1F("hp_m_unwgt_minusrun2","",
    n_varp_mbins, p_m_bin_edges);
```

```
file2 ->cd ( ) ;
file2 ->GetObject ( " hp_m_sin_phi_plus4 " , " hp_m_sin_phi_plusrun2 " ) ;
file2 ->GetObject ( " hp_m_unwgt_plus4 " , " hp_m_unwgt_plusrun2 " ) ;
file2 ->GetObject ( " hp_m_sin_phi_minus4 " , " hp_m_sin_phi_minusrun2 " ) ;
file2 ->GetObject ( " hp_m_unwgt_minus4 " , " hp_m_unwgt_minusrun2 " ) ;


//copy run3

TH1F *hp_m_sin_phi_plusrun3 = new TH1F(" hp_m_sin_phi_plusrun3 " , " " ,
    n_varp_mbins , p_m_bin_edges ) ;
TH1F *hp_m_unwgt_plusrun3 = new TH1F(" hp_m_unwgt_plusrun3 " , " " ,
    n_varp_mbins , p_m_bin_edges ) ;
TH1F *hp_m_sin_phi_minusrun3 = new TH1F(" hp_m_sin_phi_minusrun3 " , " " ,
    n_varp_mbins , p_m_bin_edges ) ;
TH1F *hp_m_unwgt_minusrun3 = new TH1F(" hp_m_unwgt_minusrun3 " , " " ,
    n_varp_mbins , p_m_bin_edges ) ;

file3 ->cd ( ) ;
file3 ->GetObject ( " hp_m_sin_phi_plus4 " , " hp_m_sin_phi_plusrun3 " ) ;
file3 ->GetObject ( " hp_m_unwgt_plus4 " , " hp_m_unwgt_plusrun3 " ) ;
file3 ->GetObject ( " hp_m_sin_phi_minus4 " , " hp_m_sin_phi_minusrun3 " ) ;
file3 ->GetObject ( " hp_m_unwgt_minus4 " , " hp_m_unwgt_minusrun3 " ) ;


//copy run4


TH1F *hp_m_sin_phi_plusrun4 = new TH1F(" hp_m_sin_phi_plusrun4 " , " " ,
    n_varp_mbins , p_m_bin_edges ) ;
TH1F *hp_m_unwgt_plusrun4 = new TH1F(" hp_m_unwgt_plusrun4 " , " " ,
    n_varp_mbins , p_m_bin_edges ) ;
TH1F *hp_m_sin_phi_minusrun4 = new TH1F(" hp_m_sin_phi_minusrun4 " , " " ,
    n_varp_mbins , p_m_bin_edges ) ;
TH1F *hp_m_unwgt_minusrun4 = new TH1F(" hp_m_unwgt_minusrun4 " , " " ,
    n_varp_mbins , p_m_bin_edges ) ;

file4 ->cd ( ) ;
file4 ->GetObject ( " hp_m_sin_phi_plus4 " , " hp_m_sin_phi_plusrun4 " ) ;
file4 ->GetObject ( " hp_m_unwgt_plus4 " , " hp_m_unwgt_plusrun4 " ) ;
file4 ->GetObject ( " hp_m_sin_phi_minus4 " , " hp_m_sin_phi_minusrun4 " ) ;
file4 ->GetObject ( " hp_m_unwgt_minus4 " , " hp_m_unwgt_minusrun4 " ) ;

//copy run5

TH1F *hp_m_sin_phi_plusrun5 = new TH1F(" hp_m_sin_phi_plusrun5 " , " " ,
    n_varp_mbins , p_m_bin_edges ) ;
```

```
TH1F *hp_m_unwgt_plusrun5 = new TH1F("hp_m_unwgt_plusrun5","",
    n_varp_mbins,p_m_bin_edges);
TH1F *hp_m_sin_phi_minusrun5 = new TH1F("hp_m_sin_phi_minusrun5","",
    n_varp_mbins,p_m_bin_edges);
TH1F *hp_m_unwgt_minusrun5 = new TH1F("hp_m_unwgt_minusrun5","",
    n_varp_mbins,p_m_bin_edges);

file5->cd();
file5->GetObject("hp_m_sin_phi_plus4","hp_m_sin_phi_plusrun5");
file5->GetObject("hp_m_unwgt_plus4","hp_m_unwgt_plusrun5");
file5->GetObject("hp_m_sin_phi_minus4","hp_m_sin_phi_minusrun5");
file5->GetObject("hp_m_unwgt_minus4","hp_m_unwgt_minusrun5");

//target hists

TH1F *hp_m_sin_phi_plusbin1 = new TH1F("hp_m_sin_phi_plusbin1
    ","",1,0.0,0.05);
TH1F *hp_m_unwgt_plusbin1 = new TH1F("hp_m_unwgt_plusbin1
    ","",1,0.0,0.05);
TH1F *hp_m_sin_phi_minusbin1 = new TH1F("hp_m_sin_phi_minusbin1
    ","",1,0.0,0.05);
TH1F *hp_m_unwgt_minusbin1 = new TH1F("hp_m_unwgt_minusbin1
    ","",1,0.0,0.05);

//bin1

TH1F *h1d_bin1 = new TH1F("h1d_bin1","Sin(#phi) weighted distribution
    for positive helicity",1,0.0,0.05);
TH1F *h2d_bin1 = new TH1F("h2d_bin1","Sin(#phi) weighted distribution
    for negative helicity",1,0.0,0.05);
h1d_bin1.Sumw2();
h2d_bin1.Sumw2();
h1d_bin1.Divide(hp_m_sin_phi_plusrun5, hp_m_unwgt_plusrun5);
h2d_bin1.Divide(hp_m_sin_phi_minusrun5, hp_m_unwgt_minusrun5);
TH1F *h12d_bin1 = new TH1F("h12d_bin1","A_{LT}'",1,0.0,0.05);
h12d_bin1.Sumw2();
h12d_bin1.Add(h1d_bin1,h2d_bin1,0.9936,-1.0);
Double_t binContent = h->GetBinContent(bin);
cout<<binContent;
```

Appendix D

A small part of the QUEEG Perl script. These parts are my contribution to the script.
Part 1:

```
// assume the missing momentum will satisfy the calina cut where we
    decide below whether or not
// to keep the event if the missing momentum is large enough. This is
    a ploy to populate high
// missing momentum events more.

below_p_m_threshold = 1;

while (below_p_m_threshold==1) {
  //pick fermi momentum in lab frame and direction from xsec table.
  // modified to get more high pfermi events above some threshold.
//    big_enough = 0;
//    if(htype == PROTON){
//      while (big_enough == 0){
//      weight_table_proton->GetRandom2(cos_theta, pfermi);
//      if (pfermi > 0.0) {
//        big_enough=1;
//        //cout << "p_fermi = " << pfermi << endl;
//      }
//      }
//    } else{
//      weight_table_neutron->GetRandom2(cos_theta, pfermi);
//    }
    if(htype == PROTON){
      weight_table_proton->GetRandom2(cos_theta, pfermi);
    } else{
      weight_table_neutron->GetRandom2(cos_theta, pfermi);
    }
    sin_theta = sqrt(1 - cos_theta*cos_theta);
    phi = 2*PI*rand->Rndm();
    pfermi3.z = pfermi*cos_theta;
    pfermi3.x = pfermi*sin_theta*cos(phi);
    pfermi3.y = pfermi*sin_theta*sin(phi);

    //pick scattered electron dir
    theta_rf = get_electron_angle(htype, pfermi, acos(cos_theta));
    theta = calc_theta_lab(init_energy, pfermi, acos(cos_theta), theta_rf)
        ;
```

Part 2:

```
 // put in the calina's cut here.

  // get p_m in order to apply the cut on it to get more events at
      large p_m (calina cut).
  beam.SetPxPyPzE(0,0,init_energy,init_energy);
  tgt.SetPxPyPzE(0.0,0.0,0.0,Md); // set the mass of the deuteron tgt
      here.
  e_scatt.SetPxPyPzE(e_out3.x, e_out3.y, e_out3.z, Eprime);
  proton4vec.SetPxPyPzE(nuc3.x, nuc3.y, nuc3.z, sqrt(pow(nuc3mag,2) +
      pow(Mp,2)) );

  missing4vec = beam + tgt - e_scatt - proton4vec;
  missing3vec = missing4vec.Vect();
  missing3vec_mag = missing3vec.Mag();
  p_m = missing3vec_mag;
  if (p_m < p_mlo) {
  below_p_m_threshold = 1;
    //cout << "p_m = " << p_m << " missed the cut." << endl;
  continue;
   } else {
   below_p_m_threshold = 0;
    //cout << "p_m = " << p_m << " threshold= " << p_mlo << endl;
      }   // end of test on p_m.
 } // end of loop over p_m attempts.

//cout << "p_m = " << p_m << " end of looplstlisting." << endl;

//fill diagnostic histograms
scattered_theta = acos(e_hat.z);
nucleon_theta = acos(nuc_hat.z);
Qsq = 4*init_energy*Eprime*pow(sin(scattered_theta/2.0),2.0);
nu = init_energy - Eprime;
wsq = M_nucleon*M_nucleon - Qsq +2*M_nucleon*nu;
if(htype == PROTON){
  qsq_proton->Fill(Qsq);
} else{
  qsq_neutron->Fill(Qsq);
}
```

Appendix E

This is the Mathematica file for the reversed torus polarity data set used to obtain reduced χ^2. A similar file exists for the normal torus polarity data set.

(*acc $-$ 4/6/09CHISQUAREDNBFORGPGALTp*)
Clear[x];
(*$\chi^2 = \sum \frac{(MC_i - <curve_i>)^2}{\sigma_i{}^2} \frac{1}{N_{DOF}}$, where$\sigma_i$istheMC$_i$uncertainty*)
$n = 8$;

(*N_{DOF} = #points $-$ fitparameters = $8 - 0 = 8$*)
$f[x\_] := -\frac{((-0.0652557*x\char`^2)+(0.503095*x\char`^4))}{(1+(-11.0388*x)+(36.0937*x\char`^2)+(-126.685*x\char`^4)+(256.143*x\char`^6))}$;
(*calina$'$sfitfunction*)
(*NBbinsrunfrom0to13 $-$ thelatterhavenocontent*)
(* BIN 1 *)
Clear[x]; Clear[x0]; Clear[x1];
mc1 $= 0.00164308; \delta$mc1 $= 0.00119103; $x0 $= 0.0; $x1 $= 0.050$;
avgcurve1 $= \frac{\text{Integrate}[f[x],\{x,x0,x1\}]}{x1-x0}$;
χsquared1 $= \frac{(mc1-avgcurve1)^2}{\delta mc1^2}$
1.71073
(*NBbinsrunfrom0to13 $-$ thelatterhavenocontent*)
(* BIN 2 *)
Clear[x]; Clear[x0]; Clear[x1];
mc2 $= 0.000755774; \delta$mc2 $= 0.00140182; $x0 $= 0.050; $x1 $= 0.100$;
avgcurve2 $= \frac{\text{Integrate}[f[x],\{x,x0,x1\}]}{x1-x0}$;
χsquared2 $= \frac{(mc2-avgcurve2)^2}{\delta mc2^2}$
0.0561293
(*NBbinsrunfrom0to13 $-$ thelatterhavenocontent*)
(* BIN 3 *)
Clear[x]; Clear[x0]; Clear[x1];
mc3 $= 0.00239838; \delta$mc3 $= 0.00284316; $x0 $= 0.100; $x1 $= 0.150$;
avgcurve3 $= \frac{\text{Integrate}[f[x],\{x,x0,x1\}]}{x1-x0}$;
χsquared3 $= \frac{(mc3-avgcurve3)^2}{\delta mc3^2}$
1.99533
(* BIN 4 *)
Clear[x]; Clear[x0]; Clear[x1];
mc4 $= 0.0221362; \delta$mc4 $= 0.00535747; $x0 $= 0.150; $x1 $= 0.200$;
avgcurve4 $= \frac{\text{Integrate}[f[x],\{x,x0,x1\}]}{x1-x0}$
0.0246153
Integrate[$f[x], \{x, x0, x1\}$]
0.00123076
χsquared4 $= \frac{(mc4-avgcurve4)^2}{\delta mc4^2}$

0.214121

(* BIN 5 *)

Clear[x]; Clear[x0]; Clear[x1];

mc5 $= 0.0290465; \delta$mc5 $= 0.00924209;$ x0 $= 0.200;$ x1 $= 0.250;$

avgcurve5 $= \frac{\text{Integrate}[f[x],\{x,\text{x0},\text{x1}\}]}{\text{x1}-\text{x0}};$

χsquared5 $= \frac{(\text{mc5}-\text{avgcurve5})^2}{\delta\text{mc5}^2}$

0.806177

(* BIN 6 *)

Clear[x]; Clear[x0]; Clear[x1];

mc6 $= 0.005432; \delta$mc6 $= 0.0126138;$ x0 $= 0.250;$ x1 $= 0.350;$

avgcurve6 $= \frac{\text{Integrate}[f[x],\{x,\text{x0},\text{x1}\}]}{\text{x1}-\text{x0}};$

χsquared6 $= \frac{(\text{mc6}-\text{avgcurve6})^2}{\delta\text{mc6}^2}$

1.0657

(* BIN 7 *)

Clear[x]; Clear[x0]; Clear[x1];

mc7 $= -0.0437412; \delta$mc7 $= 0.024967;$ x0 $= 0.350;$ x1 $= 0.550;$

avgcurve7 $= \frac{\text{Integrate}[f[x],\{x,\text{x0},\text{x1}\}]}{\text{x1}-\text{x0}};$

χsquared7 $= \frac{(\text{mc7}-\text{avgcurve7})^2}{\delta\text{mc7}^2}$

0.95288

(* BIN 8 *)

Clear[x]; Clear[x0]; Clear[x1];

mc8 $= 0.136036; \delta$mc8 $= 0.112876;$ x0 $= 0.550;$ x1 $= 0.700;$

avgcurve8 $= \frac{\text{Integrate}[f[x],\{x,\text{x0},\text{x1}\}]}{\text{x1}-\text{x0}};$

χsquared8 $= \frac{(\text{mc8}-\text{avgcurve8})^2}{\delta\text{mc8}^2}$

1.74132

chisquaredfinal $=$

(χsquared1 $+ \chi$squared2 $+ \chi$squared3 $+ \chi$squared4 $+ \chi$squared5 $+ \chi$squared6 $+ \chi$squared7$+$ χsquared8)/8

1.0678